Quaternary Science Reviews 115 (2015) 132–142

Contents lists available at ScienceDirect

Quaternary Science Reviews

journal homepage: www.elsevier.com/locate/quascirev

Astronomical and glacial forcing of East Asian summer monsoon variability

Youbin Sun [a, b, *], John Kutzbach [c, **], Zhisheng An [a, b], Steven Clemens [d], Zhengyu Liu [c], Weiguo Liu [a], Xiaodong Liu [a], Zhengguo Shi [a], Weipeng Zheng [e], Lianji Liang [a], Yan Yan [a], Ying Li [a]

[a] State Key Laboratory of Loess and Quaternary Geology, Institute of Earth Environment, Chinese Academy of Sciences, Xi'an 710061, China
[b] Joint Center for Global Change Studies, Beijing 100875, China
[c] Center for Climatic Research, University of Wisconsin-Madison, Madison, WI 53706, USA
[d] Department of Earth, Environmental and Planetary Sciences, Brown University, Providence, RI 02912-1846, USA
[e] Institute of Atmospheric Physics, Chinese Academy of Sciences, Beijing 100029, China

ARTICLE INFO

Article history:
Received 19 November 2014
Received in revised form
11 March 2015
Accepted 13 March 2015
Available online

Keywords:
Chinese loess
East Asian summer monsoon
Insolation
Ice-sheets
CO_2
Variability and dynamics

ABSTRACT

The dynamics of glacial–interglacial monsoon variability can be attributed to orbitally induced changes in summer insolation and internal boundary conditions. However, the relative impacts of astronomical and internal factors on East Asian summer monsoon variability remain controversial. Here we combine proxy data and model results to evaluate the response of East Asian summer monsoon change to these forcings. $\delta^{13}C$ of loess carbonate, a sensitive summer monsoon proxy from the western Chinese Loess Plateau, demonstrates coexistence of distinct 100-, 41- and 23-ka periods, in contrast to precession-dominated speleothem $\delta^{18}O$ records in South China. Model results indicate that insolation, ice and CO_2 have distinct impacts on summer precipitation changes in East Asia, whereas their relative impacts are spatially different, with a relatively stronger insolation effect in south China and a more dominant ice/CO_2 influence in north China. Combined proxy data and model results indicate that East Asian summer monsoon variability was induced by integrated effects of summer insolation and changing boundary conditions (e.g., ice sheets and CO_2 concentration). Our proxy-model comparison further suggests that gradual weakening of the summer monsoon related to slowly decreasing summer insolation at astronomical timescales will be likely overwhelmed by the projected ongoing anthropogenic CO_2 emissions.

1. Introduction

Investigating the hydrological cycle is essential for a sustainable Future Earth, because water plays a critical role in global ecological and social systems. Monsoon circulation, as a primary driver of hydrological changes in the low-to-mid latitudes of both hemispheres (Webster et al., 1998; Wang and Ding, 2008; Wang, 2009; Guo et al., 2012; Liu et al., 2013; An et al., 2015), can seriously impact food production, water supply, and natural hazards through severe flood and drought events (Ding and Chan, 2005; Huang et al., 2007). Therefore, understanding monsoon variability from the natural past to the anthropogenic future is critical for both scientific communities and policy makers. Investigation of the natural variability and dynamics of monsoon-related hydrological changes has improved greatly through paleoclimate modeling and data-model integration studies over past decades (e.g., Kutzbach and Street-Perrott, 1985; Kutzbach and Guetter, 1986; Prell and Kutzbach, 1992; Braconnot et al., 2007; Kutzbach et al., 2008; Liu et al., 2014). However, assessing the relative importance of astronomical and glacial factors on monsoon variability remains challengeable due to varied sensitivity of both models and proxies to these forcings (Ding et al., 1995; Wang et al., 2008b; Lu et al., 2013; Liu et al., 2014).

Although monsoon circulation is often defined as a seasonal change in prevailing wind directions, many monsoonal regions also experience large seasonal differences in rainfall as well (Webster

* Corresponding author. State Key Laboratory of Loess and Quaternary Geology, Institute of Earth Environment, Chinese Academy of Sciences, Xi'an 710075, China.
** Corresponding author. Center for Climatic Research, University of Wisconsin-Madison, Madison, WI 53706, USA.
E-mail addresses: sunyb@ieecas.cn (Y. Sun), jek@wisc.edu (J. Kutzbach).

http://dx.doi.org/10.1016/j.quascirev.2015.03.009
0277-3791/

et al., 1998; Wang and Ding, 2008). Geologically, many proxy indicators of paleomonsoon variability reflect some aspect of changes in rainfall and wind, such as Chinese loess and speleothem records (e.g., Maher and Thompson, 1995; An, 2000; Wang et al., 2008b; Cheng et al., 2009; Liu et al., 2014). Notably, these monsoonal proxies display a considerable range of variability in amplitude, phasing (timing), and relative concentrations of variance within the primary frequency bands associated with three earth's orbital parameters (eccentricity, obliquity, and precession) (e.g., Clemens et al., 2010; An et al., 2011; 2015; Wang et al., 2014). For example, most loess-based proxies are characterized by distinct glacial–interglacial variations with a dominant 100-ka cycle over the last 800 ka, implying a strong coupling to change in ice-sheet volume (Ding et al., 1995; Liu et al., 1999). In contrast, speleothem $\delta^{18}O$ shows a dominant 23-ka cycle, suggesting a direct link to insolation forcing (Wang et al., 2008b; Cheng et al., 2009, 2012). More recently, further analysis of the spelethom records to ice-sheets and insolation forcing indicates a distinct influence of the ice volume change on the $\delta^{18}O$ variability (Caballero-Gill et al., 2012; Thomas et al., 2014; Cai et al., 2015). Different responses of these proxies make it challenging to pin down the relative sensitivity of Asian summer monsoon change to insolation and glacial forcing.

A robust evaluation of the glacial/insolation impacts on monsoon changes has been made using comprehensive data-model comparisons (e.g., Kutzbach and Street-Perrott, 1985; Liu et al., 2003, 2014; Braconnot et al., 2007, 2012; Yin et al., 2009, 2014; Weber and Tuenter, 2011; Eagle et al., 2013). Here we present a sensitive summer monsoon proxy generated from two high-resolution loess sequences on the northwestern Chinese Loess Plateau (CLP), which demonstrates strong sensitivity of summer monsoon variability to changing insolation and glacial boundary conditions. The relative impacts of insolation, ice and CO_2 on East Asian summer monsoon variability were evaluated using sensitivity experiments with the Community Climate System Model 3 (CCSM3) (Collins et al., 2006; Meehl et al., 2006). Further comparison of paleoclimate data with modeling results indicates that insolation, ice and CO_2 have varying contributions to summer precipitation changes in East Asia.

2. Monsoonal setting in East Asia

Monsoon circulation is characterized by seasonal changes in wind direction and precipitation (Webster et al., 1998). Today, monsoonal wind and precipitation are highly seasonal in East Asia. In summer (hereafter referred to as the rainy season from May to September), warm and humid air originating from low-latitude oceans is transported northwestward up to the China–Mongolia boundary, resulting in strong monsoonal precipitation in East Asia (Gao et al., 1962). The northern boundary of the summer monsoon front roughly corresponds to the isohyetal line of mean summer precipitation (SP) around 1 mm/day (Fig. 1a). From a modern meteorological perspective, changes in southerly wind intensity, sea level pressure and summer precipitation within a certain domain can be employed as monsoonal proxies (Wang et al., 2008a). However, monsoonal precipitation is highly variable in East Asia because of meridional shifts in the rain belt linked to variability of the North Pacific Subtropical High (Ding and Chan, 2005), leading to a demarcation of climate regimes between north and south China at ~33°N (Ding and Chan, 2005; Ding et al., 2008). Over the past 50 years (1960–2010), SP has decreased in most parts of north China, but increased evidently in southeast China (Fig. 1b), implying that the SP change cannot be used straightforward to indicate the summer monsoon intensity.

Among available monsoon proxies, seasonality of wind and precipitation changes are two widely used indicators to define the tempo-spatial variation of the summer monsoon intensity (Li and Zeng, 2002; Wang and Ding, 2008). However, correlation between monsoonal winds and precipitation is complicated in East Asia (Fig. 1c). In most parts of north China including the CLP, a decreasing trend of the SP over the last 50 years is positively correlated with weakening of the monsoonal wind intensity defined as a dynamical normalized wind seasonality index (Li and Zeng, 2002). In south China, particularly over the middle and lower reaches of the Yangtze River, however, summer precipitation increases gradually over the last 50 years due to the southward shift of the monsoonal rain belt, and is negatively correlated with weakening of the monsoonal wind intensity. An anti-phase response of regional summer precipitation change to insolation forcing between north and south China was also identified in the transient simulations (Shi et al., 2012; Liu et al., 2014). A continuous simulation of the East Asian monsoon (EAM) revealed that from the LGM to Holocene maximum, an enhanced southerly monsoon wind is accompanied by an increased monsoon rainfall in north China, but not significant rainfall changes in southeastern China, implying that the precipitation change in north China is positively related to the monsoon intensity (Liu et al., 2014).

From a paleomonsoon perspective, it's difficult to infer the summer monsoonal wind intensity from geological archives. Most understanding of summer monsoon intensity is based on the precipitation-related proxies derived from pedogenic intensity of Chinese loess and isotopic composition of speleothems, although the extent to which these proxies can be interpreted as a pure summer monsoon indicator is still debated (Wang et al., 2001, 2008b; Cheng et al., 2009, 2012; Clemens et al., 2010; Dayem et al., 2010; Pausata et al., 2011; Maher and Thompson, 2012). Recently, comparison of observation data and isotope modeling results suggests that the strong summer monsoon can be characterized by intensified southerly wind, corresponding well to negative $\delta^{18}O$ over China and enhanced rainfall in northern China (Liu et al., 2014). Therefore, the paleo-precipitation change in northern China, including loess-based precipitation proxies on the CLP, most likely reflects the summer monsoon variation.

3. Material and methods

Two loess sequences at Jingyuan (JY, 36°20′30″N, 104°37′24″E) and Gulang (GL, 37°28′43″N, 102.52′28″E) are located in the northwestern CLP, close to the northern limit of the summer monsoon front (Fig. 1a). SP at these two sites contributes to 75% of the annual precipitation over the past 50 years, with ~60% water vapor transported by the southerly monsoonal wind (Yan et al., 2013). High sedimentation rate and weakly weathered loess sequences at the northwestern CLP can resolve millennial through glacial–interglacial monsoon variability (Sun et al., 2010, 2012b). Samples at 10-cm intervals were collected from the upper 110 m of two profiles including two 20-m loess pits in the uppermost part for measurements of magnetic susceptibility (χ), grain size and carbon isotopes of inorganic carbonates ($\delta^{13}C_{IC}$). Grain size distribution was determined using a Malvern 2000 laser instrument after removal of organic matter and carbonate. Magnetic susceptibility was measured with a Bartington MS 2 m. Carbon and Oxygen isotopes of inorganic carbonate of loess samples were measured using an isotope ratio mass spectrometer (MAT-252) with an automated carbonate preparation device (Kiel II). Standard deviation of carbon isotopic results is smaller than ±0.1‰ estimated from repeated analyses of the laboratory standards.

The response of monsoon circulation to insolation and glacial forcing is not consistent in different models, particularly the

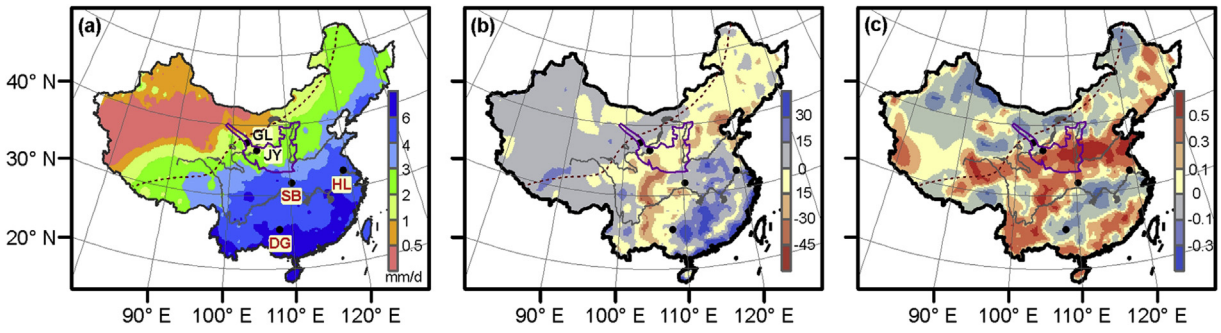

Fig. 1. (a) Summer precipitation (May to September, mm/day) and locations of Chinese loess and cave sites; (b) Trend (mm/10 years) of summer precipitation change over 1961–2010 (data from China meteorological data center); (c) Correlation coefficients between changes in summer precipitation and monsoonal wind index (Li and Zeng, 2002). Two loess sections (GL-Gulang, JY-Jingyuan) are located in the northwestern Chinese Loess Plateau. Three caves (SB-Sanbao, HL-Hulu, DG-Dongge) are situated in south China. Brown dotted line denotes the northern limit of the summer monsoon front inferred from meteorological observations (Gao et al., 1962). (For interpretation of the references to color in this figure legend, the reader is referred to the web version of this article.)

monsoonal rainfall change in East Asia (Jiang et al., 2011; Zhao and Harrison, 2012). Comparison of simulated and reconstructed precipitation changes in East Asia suggests that the CCSM3 (a coupled ocean-atmosphere model) can be applied well for simulating the seasonal cycle of monsoon circulation and precipitation in East Asia (Meehl et al., 2006; Otto-Bliesner et al., 2006; Braconnot et al., 2007). Comparison of CCSM3 simulated results with the reanalysis data suggests consistent features such as seasonal shift of the wind direction and precipitation and spatial distribution of the rainfall in East Asia (Supplementary Fig. S1). More information about the performance of the CCSM3 model for simulating Asian paleoclimate changes were detailed in Otto-Bliesner et al. (2006) and Meehl et al. (2006).

Three sensitivity experiments in this study were conducted by the CCSM3 to evaluate the response of the Asian monsoon for the pre-industrial (PI, 0 ka), Early Holocene (EH, 9 ka) and the Last Glacial Maximum (LGM, 21 ka). Two additional experiments, LGM condition with PI ice-sheets ($LGM_{PI\text{-}ICE}$) and with PI CO_2 concentration ($LGM_{PI\text{-}CO2}$), are carried out in order to evaluate the effects of changing ice-sheets and CO_2 concentration in glacial period. The experimental design generally follows the framework of the Paleoclimate Modelling Intercomparison Project phase 3 (PMIP3), except that the mid-Holocene (MH, 6 ka BP) experiment is replaced by the early-Holocene (EH, 9 ka BP). For the PI experiment, all the boundary conditions are kept as present-day and the CO_2 concentration is set to 280 ppmv. In EH experiment, only the astronomical parameters are changed (Berger, 1978). In LGM experiment, the distribution and height of the ice sheets are from ICE-5G dataset (Peltier, 2004) and the CO_2 concentration is 185 ppmv (Pertit et al., 1999). The $LGM_{PI\text{-}ICE}$ and $LGM_{PI\text{-}CO2}$ experiments were designed by removing the excess LGM ice sheets (compared to PI with ice sheets only in Greenland and Antarctica) and of using PI greenhouse gas forcing (compared to the lowered LGM greenhouse gases). The astronomical parameters and boundary conditions for each experiment are listed in Table 1. These experiments were run for 100 years and the results are integrated for last 20 years at an atmospheric horizontal resolution of 2.8° × 2.8°. To evaluate the spatial difference in the impacts of astronomical and glacial forcing, the summer precipitation are averaged over north China (NC, 33–42°N, 100–120°E) and south China (SC, 24–33°N, 100–120°E), respectively.

4. Grain size age model

Chronologies of Chinese loess-paleosol sequences have been generated using magnetic susceptibility-based model (Kukla et al., 1988), grain-size model (Porter and An, 1995; Vandenberghe et al., 1997), and astronomical calibration (Ding et al., 1994, 2002; Lu et al., 1999; Heslop et al., 2000; Sun et al., 2006). High correlation between loess grain size and benthic $\delta^{18}O$ records implies a strong coupling between the winter monsoon and ice volume changes (Ding et al., 1995, 2002; Liu et al., 1999; Hao et al., 2012), which allows establishing the chronology of Chinese loess by correlation of mean grain size with the benthic $\delta^{18}O$ stack (Lisiecki and Raymo, 2005). Abrupt methane and speleothem $\delta^{18}O$ changes are contemporaneous with high-latitude cooling during glacial terminations (Cheng et al., 2009), confirming a strong coupling of rapid monsoon and ice volume changes during deglaciations. Thus, ages of the glacial terminations and interglacial–glacial transitions inferred from the benthic $\delta^{18}O$ can be adopted as time controls for generating the loess chronology (Porter and An, 1995; Hao et al., 2012).

Since grain size fluctuations within the upper 110 m (S_0-L_4) at GL and JY loess sections correspond well to benthic $\delta^{18}O$ record over the last 350 ka (Lisiecki and Raymo, 2005), eleven tie points were selected to match rapid changes of the grain size and benthic $\delta^{18}O$ during the boundaries of marine isotope stages (MIS) 1–10 (Fig. 2). Five additional age markers from the top 20-m (loess pits) at GL and JY were obtained by OSL dating (Sun et al., 2012b). Due to the coeval changes between sedimentation rate and grain size (Ding et al.,

Table 1
Earth's orbital parameters (Berger, 1978), CO_2 concentration (Pertit et al., 1999), ice-sheets and topography (Peltier, 2004) in the CCSM3 sensitivity experiments and the PMIP3 models. Also shown are the modeled summer precipitation (SP) in north China (NC, 33–42°N, 100–120°E) and South China (SC, 24–33°N, 100–120°E) from the CCSM3 results.

Experiments	Topography	Ice-sheets	CO_2 (ppmv)	E	T	P	SP (NC, mm/d)	SP (SC, mm/d)
PI (0 ka)	Modern	Modern	280	0.016724	23.446	102.04	3.89	5.47
EH (9 ka)	Modern	Modern	280	0.019280	24.232	311.25	4.2	6.4
LGM (21 ka)	ICE-5G	ICE-5G	185	0.018994	22.949	114.42	2.96	4.54
$LGM_{PI\text{-}ICE}$	Modern	Modern	185	0.018994	22.949	114.42	3.54	5.42
$LGM_{PI\text{-}CO2}$	ICE-5G	ICE-5G	280	0.018994	22.949	114.42	3.27	4.98

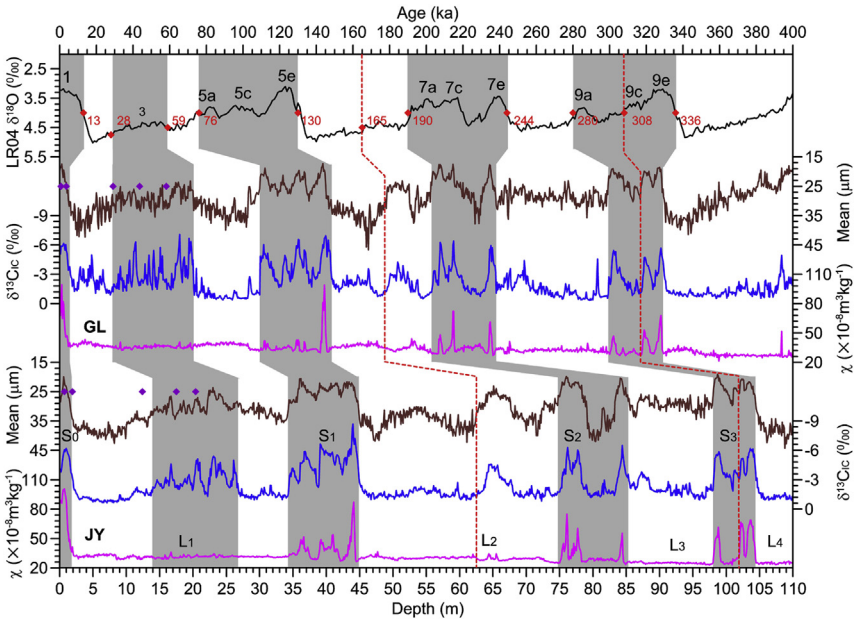

Fig. 2. Variations of magnetic susceptibility (χ, pink), mean grain size (brown) and $\delta^{13}C_{IC}$ (blue) of the GL and JY sections, and their correlation with benthic $\delta^{18}O$ stack (black, Lisiecki and Raymo, 2005). Red diamonds indicate ages derived from tie points linking rapid changes in mean grain size with the boundaries of marine isotope stages (MIS) recorded by the benthic $\delta^{18}O$ record. Red dashed lines denote two additional ages derived within MIS 6 and 9, respectively. Purple diamonds are the optically stimulated luminescence dates (Sun et al., 2012b). (For interpretation of the references to color in this figure legend, the reader is referred to the web version of this article.)

2001), the chronology can be generated using the weighted grain-size model proposed by Porter and An (1995):

$$T_m = T_1 + (T_2 - T_1)\left(\sum_{i=1}^{m} A_i^{-1}\right)\left(\sum_{i=1}^{n} A_i^{-1}\right)^{-1}$$

where T_1 and T_2 are the age control points, respectively; A_i is the sedimentation rate at depth i, which is assumed to be proportional to the mean grain size; n is the total sampling level between T_1 and T_2; and m is the sampling level at T_1 and T_2. The weighted grain size model is more reliable than those obtained by linear interpolation or by susceptibility model (Hao et al., 2012). The chronological uncertainty is less than 2 ka for these tie points and interpolated timing, respectively (Lisiecki and Raymo, 2005; Hao et al., 2012).

The grain-size age model was evaluated by comparison with previously published loess chronologies, benthic $\delta^{18}O$ stack and mean summer insolation (Fig. 3). Consistent with previous land-ocean comparisons (Liu, 1985; Bloemendal et al., 1995; Ding et al., 1995, 2002; Liu et al., 1999), the paleosol layers (S_0 to S_3) are well correlated to MIS 1 to 9, respectively. Note that grain size time series at JY and GL show three peaks in these paleosol layers, corresponding well to the precessional-scale insolation maxima (Berger, 1978; Berger et al., 2010). However, grain size records from the central CLP exhibit insignificant variability in these paleosols, due to relatively low sedimentation rates and strong pedogenesis (Ding et al., 2002; Sun et al., 2006; Hao et al., 2012). Chronologies of S_0 to S_2 are consistent among these loess age models, whereas the timing of L_2 and S_3 is different in these age models. Three grain size peaks in S_3 are well correlated to precessional insolation maxima and MIS 9 in our age models, consistent with the astronomical timescale developed by Sun et al. (2006). In two other age models (Ding et al., 2002; Hao et al., 2012), however, the S_3 was compressed and correlated to early MIS 9 (~305–336 ka), whilst L_2 was expanded to MIS8 (245–280 ka) and late MIS 9 (280–305 ka). Clearly, our grain size time series reveal a good land-ocean matching for the glacial–interglacial climate fluctuations.

5. Results and discussion

5.1. Sensitivity of loess proxies to monsoon variability

Mean grain size, χ, and $\delta^{13}C_{IC}$ exhibit almost identical fluctuations at JY and GL, demonstrating robust inter-profile reproducibility (Fig. 2). Loess grain size mainly reflects the energy of winds that transport dust particles from source areas to the CLP and thus has been widely employed as a proxy indicator for the winter monsoon intensity (e.g., An et al., 1991; Xiao et al., 1995). Magnetic susceptibility (χ) enhancements in Chinese loess derive mainly from the pedogenic formation of fine-grained magnetic minerals during warm and humid periods (Zhou et al., 1990), and can be used to quantify the amount of paleorainfall (an indicator of the summer monsoon intensity), when the mean annual precipitation varies from 200 mm to 1200 mm (Maher and Thompson, 1995; Han et al., 1996). Since the vegetation in the western CLP is dominated by C3 plants, carbon isotopes of inorganic carbonate ($\delta^{13}C_{IC}$) is thus very sensitive to change in the precipitation-controlled vegetation density and can serve as a more reliable proxy of the summer monsoon intensity (Liu et al., 2011).

Different fluctuations between loess $\delta^{13}C_{IC}$ and magnetic susceptibility during glacial periods confirm that loess $\delta^{13}C_{IC}$ is more sensitive to precipitation change than is magnetic susceptibility (Fig. 2). The magnetic susceptibly variation is more significant in interglacial paleosols (S_0–S_3) than in glacial loess (L_1–L_4), whereas the mean grain size is less variable during interglacials compared to glacials; both are in contrast to large-amplitude $\delta^{13}C_{IC}$ fluctuations during both glacial and interglacial periods. Unlike magnetic susceptibility, that is less sensitive to glacial summer monsoon intensity in the northwestern CLP, $\delta^{13}C_{IC}$ remains sensitive to change in precipitation-controlled vegetation density (Liu et al., 2011). To evaluate the relationship between loess $\delta^{13}C_{IC}$ and summer

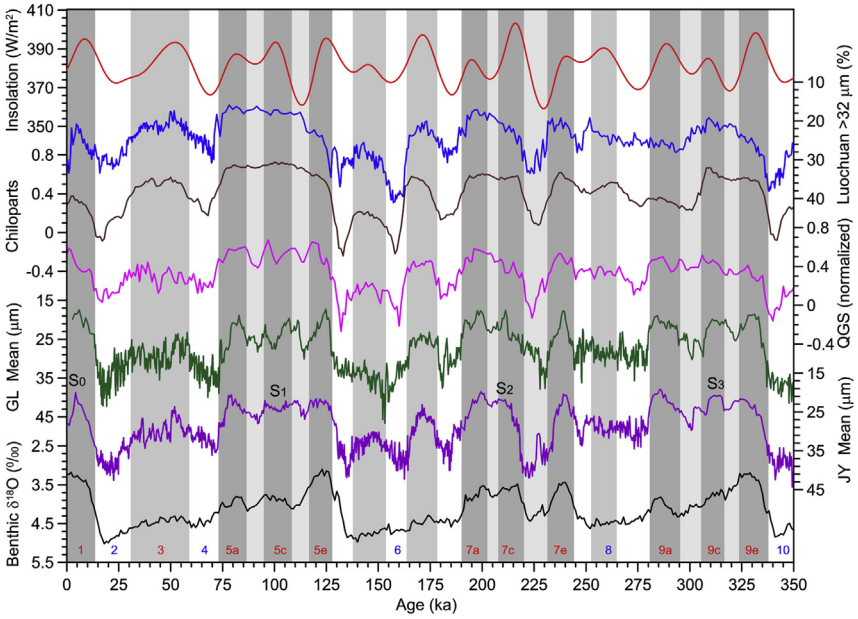

Fig. 3. Comparison of GL (green) and JY (purple) grain size time series with previously published grain size variations (Chiloparts (brown, Ding et al., 2002)); Quartz grain size (QGS, pink, Sun et al., 2006); Luochuan >32 μm content (blue, Hao et al., 2012), mean summer insolation at 65°N (red) (Berger et al., 2010), and benthic $\delta^{18}O$ stack (black) (Lisiecki and Raymo, 2005). (For interpretation of the references to color in this figure legend, the reader is referred to the web version of this article.)

precipitation change, thirteen surface soil samples were collected across the CLP, with the summer precipitation (SP) decreasing from 450 mm to 75 mm and the summer temperature changing from 23.5 to 17.5 °C (Fig. 4a). $\delta^{13}C_{IC}$ of thirteen surface samples are highly correlated with changes in precipitation, evaporation, and relative humidity during the vegetation growing season (May to September) (Fig. 4b), but less sensitive to the summer temperature changes (particularly in the western CLP), implying that the $\delta^{13}C_{IC}$ is very sensitive to the SP change.

The carbon isotope composition of inorganic carbonate in Chinese loess has been investigated intensively to indicate monsoon-induced changes in types and density of paleovegetation (e.g., Frakes and Sun, 1994; Han et al., 1997; Wang and Follmer, 1998; Ding and Yang, 2000; An et al., 2005; Sun et al., 2012a; Yang et al., 2012). However, debates still exist regarding the interpretation of bulk loess $\delta^{13}C_{IC}$, because both detrital and pedogenic carbonates are presented in Chinese loess (Liu, 1985; Ning et al., 2006; Rao et al., 2006; Sheng et al., 2008; Liu et al., 2011; Li et al., 2013). Therefore, glacial–interglacial $\delta^{13}C_{IC}$ variations are controlled by three factors: carbon isotopes of detrital carbonate ($\delta^{13}C_{DC}$), carbon isotopes of pedogenic carbonate ($\delta^{13}C_{PC}$), and the proportions of detrital and pedogenic carbonates, which can be expressed as follows:

$$\delta^{13}C_{IC} = f \times \delta^{13}C_{PC} + (1 - f) \times \delta^{13}C_{DC}$$

where f is the proportion of pedogenic carbonate, $\delta^{13}C_{PC}$ and $\delta^{13}C_{DC}$ are carbon isotopic compositions of pedogenic and detrital carbonates, respectively. To determine the $\delta^{13}C_{DC}$, surface samples were collected from the potential Asian dust sources, including Taklimakan Desert, Qaidam Basin, and Gobi/sandy deserts in north China and south Mongolia (Fig. 4a). The $\delta^{13}C$ of inorganic carbonate in desert surface sediments ranges from −0.9 to 0.7‰ (Fig. 5a), implying that the primary carbonates are derived from marine strata with an average $\delta^{13}C$ value around 0‰ (Veizer et al., 1999). The $\delta^{13}C_{PC}$ at the Jingyuan section varies between −8.5‰ and −6.5‰ (Fig. 5a), as estimated from the carbon isotopic results of organic matter ($\delta^{13}C_{OC}$, Liu et al., 2011) by subtracting the isotopic difference (~15‰) between organic matter and pedogenic carbonate (Cerling et al., 1989). The carbon isotopic difference ($\delta^{13}C_{Diff}$)

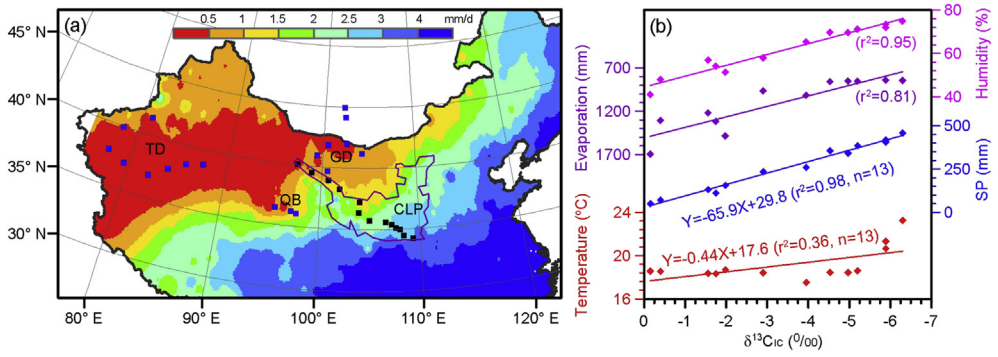

Fig. 4. (a) Summer precipitation changes (mm/day) over 1961–2000 and locations of surface samples from Asian dust sources and CLP; (b) Correlation of $\delta^{13}C_{IC}$ of surface samples from the CLP with temperature (red), precipitation (blue), evaporation (purple) and relative humidity (pink) during the summer season (May to September). TD-Taklimakan Desert; QB-Qaidam Basin; GD-Gobi Deserts in northern China and southern Mongolia, CLP-Chinese Loess Plateau. Blue and black squares denote the surface samples collected from the major Asian dust sources and CLP, respectively. (For interpretation of the references to color in this figure legend, the reader is referred to the web version of this article.)

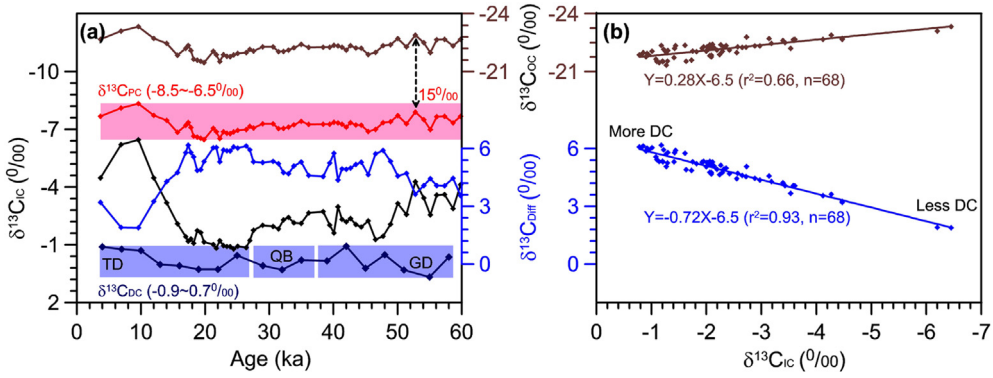

Fig. 5. (a) Glacial–interglacial variations of $\delta^{13}C_{OC}$, $\delta^{13}C_{PC}$, $\delta^{13}C_{Diff}$, and $\delta^{13}C_{IC}$, and their comparison with the $\delta^{13}C_{DC}$ results; (b) Comparison of $\delta^{13}C_{IC}$ with $\delta^{13}C_{Diff}$ and $\delta^{13}C_{OC}$. $\delta^{13}C_{PC}$ is estimated from $\delta^{13}C_{OC}$ by subtracting 15‰ (Cerling et al., 1989; Liu et al., 2011). $\delta^{13}C_{Diff}$ denotes the carbon isotopic difference between $\delta^{13}C_{PC}$ and $\delta^{13}C_{IC}$, with large difference corresponding to more proportion of detrital carbonate (DC).

between $\delta^{13}C_{IC}$ and $\delta^{13}C_{PC}$ reflects the proportional contribution of $\delta^{13}C_{DC}$ (Ning et al., 2006). Taken together, large-amplitude $\delta^{13}C_{ic}$ variability at glacial–interglacial timescales is caused by mixing ratio of detrital to pedogenic carbonates and by the $\delta^{13}C_{PC}$ variations (Fig. 5b).

In the western CLP where the vegetation is dominated by C3 plants, both $\delta^{13}C_{OC}$ variation of surface soil samples and carbon isotope composition of C3 plant are highly correlated with summer precipitation change (Wang et al., 2003; Liu et al., 2005; Rao et al., 2013). Meanwhile, high Mg/Ca and Sr/Ca ratios of authigenic carbonate at the Jingyuan section indicate that the production of pedogenic carbonate in arid CLP is heavily dependent on the precipitation-induced leaching intensity, rather than on the temperature-related evaporation (Li and Li, 2014). Therefore, both the carbon isotope and proportion of pedogenic carbonate in the arid CLP are controlled predominantly by summer precipitation change. Global satellite observations show a linear relationship between vegetation cover and precipitation under arid conditions (Donohue et al., 2013), highlighting water as the dominant limit to vegetation growth in the arid western CLP. During interglacials and interstadials, enhanced summer precipitation can result in increased soil moisture and biomass, strong soil respiration, and high pCO_2. All these conditions favor the formation of pedogenic carbonate, with more negative $\delta^{13}C$ values (Cerling, 1984; Cerling et al., 1989; Quade et al., 1989a, 1989b; An et al., 2005; Liu et al., 2011).

Although at glacial–interglacial timescales, changes in the vegetation type (C3/C4), atmospheric CO_2 and temperature might also influence the $\delta^{13}C$ values and proportion of pedogenic carbonate. These influences are rather limited compared to precipitation change, because (1) CO_2 change might lead to ~1‰ shift of carbon isotopic composition (Feng and Epstein, 1995); (2) the vegetation type in the western CLP is dominated by C3 without significant glacial–interglacial changes (Liu et al., 2011; Rao et al., 2013); and (3) impact of temperature change on the secondary carbonate production is insignificant compared to the precipitation fluctuation in the arid CLP (Li and Li, 2014). Therefore, loess $\delta^{13}C_{IC}$ variation in the northwestern CLP most likely reflects the regional precipitation change and can be regarded as a sensitive proxy for the summer monsoon intensity (Liu et al., 2011).

5.2. Glacial–interglacial summer monsoon variability

Since the $\delta^{13}C_{IC}$ variations are quite similar between GL and JY, we employed averaged $\delta^{13}C_{IC}$ result of these two sections to reflect the summer monsoon variability (Fig. 6). Given more sensitivity and higher temporal resolution relative to previous loess-based summer monsoon proxies, our $\delta^{13}C_{IC}$ record provides new insights into the summer monsoon variability over the past 350 ka. Amplitude contrast of the $\delta^{13}C_{IC}$ variations is evident (4.5–6‰) between glacials and interglacials, with more negative values during interglacials compared to glacial intervals. During three interglacials (i.e., MIS 5, 7 and 9), the $\delta^{13}C_{IC}$ record demonstrates three distinctive precessional peaks, consistent with that of both mean summer insolation and speleothem $\delta^{18}O$ records, implying a strong influence of insolation on interglacial summer monsoon variability. During glacial times, however, the $\delta^{13}C_{IC}$ amplitude is damped but still display precessional cycles, indicating a combined influence of insolation and glacial boundary conditions on the summer monsoon variability. By contrast, the speleothem $\delta^{18}O$ variations show rather uniform amplitude without significant glacial–interglacial difference. Amplitude difference between loess $\delta^{13}C_{IC}$ and speleothem $\delta^{18}O$ implies that their linkages to the summer monsoon intensity are not identical. Unlike the close link of the loess $\delta^{13}C_{IC}$ variability to the summer precipitation, the speleothem $\delta^{18}O$ in Eastern China might be influenced by multiple factors such as isotopic depletion along the vapor transport path (Hu et al., 2008; Pausata et al., 2011; Liu et al., 2014), changes in $\delta^{18}O$ values of meteoric precipitation (Wang et al., 2008b) or the amount of summer monsoon precipitation (Cheng et al., 2009), and seasonality in the amount and isotopic composition of rainfall (Clemens et al., 2010; Dayem et al., 2010; Maher and Thompson, 2012). In contrast, speleothem $\delta^{18}O$ record from southwestern China demonstrates distinctive glacial–interglacial and precessional variability, due to relatively stable moisture input and atmospheric circulation influenced by the Indian monsoon (Cai et al., 2015).

Unlike the speleothem $\delta^{18}O$ records from Hulu and Sanbao caves, the $\delta^{13}C_{IC}$ records display significant glacial–interglacial variations with strong spectral peaks at 100-, 41-, and 23-ka periods, with relative contributions of 44%, 35%, and 21%, respectively (Fig. 6b). The $\delta^{13}C_{IC}$ spectrum is in contrast to a single dominant 23-ka peak in the speleothem $\delta^{18}O$ spectrum from Eastern China and a remarkable 100-ka peak in benthic $\delta^{18}O$ and CO_2 spectra, but similar to the Indian monsoon variability inferred from the speleothem $\delta^{18}O$ record in southwestern China (Cai et al., 2015). The spectral difference implies that mechanisms driving loess $\delta^{13}C_{IC}$ and speleothem $\delta^{18}O$ variability are dissimilar. Climatically, coexistence of the 100-, 41-, and 23-ka periods in the loess $\delta^{13}C_{IC}$ spectrum is attributable to the combined influence of astronomical (i.e., summer insolation) and glacial forcing (e.g., changing surface boundary conditions such as ice volume, CO_2 concentration) (Kutzbach and Guetter, 1986; Prell and Kutzbach, 1992). The relatively strong 100-ka variance indicates a dominant glacial impact

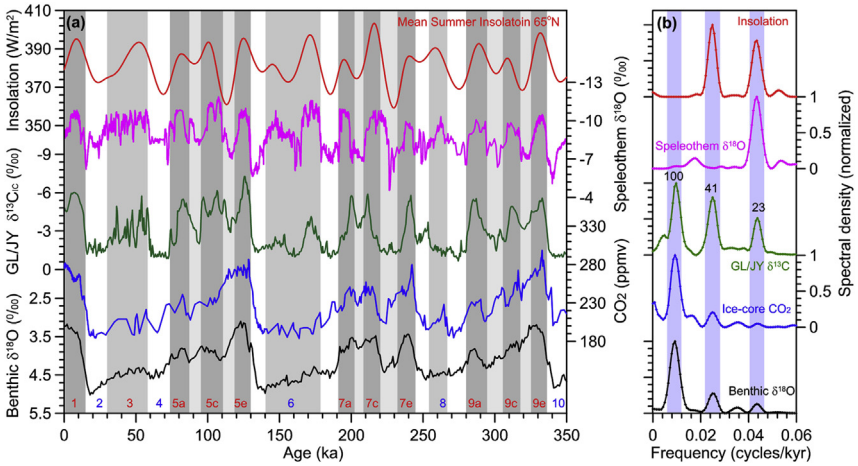

Fig. 6. Time series (a) and spectral results (b) of monsoonal proxies, summer insolation, CO_2 and benthic $\delta^{18}O$ stack. From top to bottom: (a) Mean summer insolation at 65°N (red) (Berger et al., 2010), Speleothem $\delta^{18}O$ (pink) from the Hulu and Sanbao caves (Wang et al., 2008b; Cheng et al., 2009), averaged $\delta^{13}C_{IC}$ results of GL/JY sections (green); (b) Ice-core CO_2 concentration (blue) (Pertit et al., 1999); Benthic $\delta^{18}O$ stack (black) (Lisiecki and Raymo, 2005). (For interpretation of the references to color in this figure legend, the reader is referred to the web version of this article.)

on loess $\delta^{13}C_{IC}$ variability. The obliquity and precession peaks are also distinct in the spectra of the $\delta^{13}C_{IC}$ records and mean summer insolation from May to September, but considerably weaker in the spectra of the CO_2 and benthic $\delta^{18}O$. The rainy season in East Asia is strongly associated with the onset (early May) and retreat (late September) of the summer monsoon (Gao et al., 1962; Ding and Chan, 2005; Ding et al., 2008). Thus, we propose that the total summer irradiation (a function of obliquity, Berger et al., 2010), the length of the summer season and the magnitude of summertime insolation (a function of precession and eccentricity, Berger, 1978), all might play important roles in affecting summer monsoon variability through changing land-ocean thermal contrast and meridional temperature gradient (Kutzbach and Guetter, 1986; Prell and Kutzbach, 1992; Kutzbach et al., 2008; Shi et al., 2011; Yin et al., 2014).

5.3. *Sensitivity of monsoon variability to insolation, ice and CO_2 forcing*

To identify the response of summer monsoon variability to various forcing factors, numerous sensitivity experiments with differing boundary conditions have been conducted (Kutzbach and Guetter, 1986; Prell and Kutzbach, 1992; Kutzbach et al., 2008; Weber and Tuenter, 2011; Lu et al., 2013; Liu et al., 2014). These simulations suggest that monsoonal precipitation in tropical regions respond significantly to insolation forcing, whereas changing surface boundary conditions (e.g., ice-sheets, land albedo, sea ice, and sea surface temperature) exert a strong influence on mid-latitude monsoon changes (e.g., Kutzbach and Guetter, 1986). Multi-model results suggest that both astronomical and glacial factors have distinctive impacts on Asian summer monsoon change (Yanase and Abe-Ouchi, 2007; Jiang et al., 2011) (Supplementary Fig. S2 and references therein). However, differentiating the relative influence of insolation and the coupled ice-sheet and CO_2 changes on the summer monsoon intensity remains challenging, due to the nonlinear relationship between astronomical forcing and glacial response (Hays et al., 1976; Shackleton, 2000; Yin and Berger, 2012). Here we further analyzed the modeling results of five sensitivity experiments (PI, EH, LGM, $LGM_{PI\text{-}ICE}$, and $LGM_{PI\text{-}CO2}$ in Table 1). The model results were analyzed to address the relative sensitivity of the SP change for the south and north China to the insolation, CO_2 and ice-sheet forcing, respectively.

Since the difference between the PI and EH experiments is due to the changing astronomical parameters (Table 1), the SP increase in EH relative to PI is evident in most parts of East Asia, reflecting the significant impact of insolation forcing on summer monsoon variability (Fig. 7a). The SP increase from PI to EH is largest and most significant in SC, but is also large and statistically significant in most of the eastern half of NC, compared to the region of the CLP. These spatial differences indicate that changing summer insolation has a larger influence on the SP change in SC compared to NC, because insolation-induced land-sea thermal contrast has greatest impacts in low latitudes and in areas closer to the coast (Kutzbach and Guetter, 1986). The LGM-PI difference mostly represents the impacts of increased ice-sheets (more ice at LGM than at PI) and reduced greenhouse gas (lower concentration of CO_2 at LGM relative to PI) forcing, while the effect of orbitally induced insolation forcing is small because of minor summer insolation difference between these two periods. The SP decrease from PI to LGM is significant in NC and most parts of SC, but not distinctive in southeast China (Fig. 7b). The impact of increased ice-sheets and reduced CO_2 on the SP likely derives from an increased meridional temperature gradient (Braconnot et al., 2007; Yanase and Abe-Ouchi, 2007; Jiang et al., 2011), strengthening and southward shift of the westerlies (Yanase and Abe-Ouchi, 2007; Nagashima et al., 2011), increased snow/ice cover on the Tibet Plateau (Thompson et al., 1997; Chen et al., 1999), and sea level drop during the LGM relative to the PI (Peltier, 2004; Wang et al., 2005; Jiang et al., 2011). All these factors could prevent the northwestward penetration of the summer monsoon front and thus reduce the summer precipitation amount. Our sensitivity experiments suggest significant impacts of both changing insolation and glacial boundary conditions on the summer precipitation change (Fig. 7a and b), consistent with multi-model mean results of the PMIP3 outputs (Fig. S2).

Model results of the $LGM_{PI\text{-}ICE}$ and $LGM_{PI\text{-}CO2}$ experiments were employed to evaluate the separate effect of removing the excess LGM ice sheets and of using high PI CO_2 forcing relative to the LGM condition. In general, decreased ice-sheets and increased CO_2 tend to strengthen the summer precipitation (Fig. 7c and d). In most parts of East Asia, the SP increases significantly in response to reducing ice sheet, with 0.58 mm/day and 0.88 mm/day in NC and SC, respectively; while the SP increases induced by CO_2 are 0.31 mm/day in NC and 0.44 mm/day in SC (Table 1). The CO_2

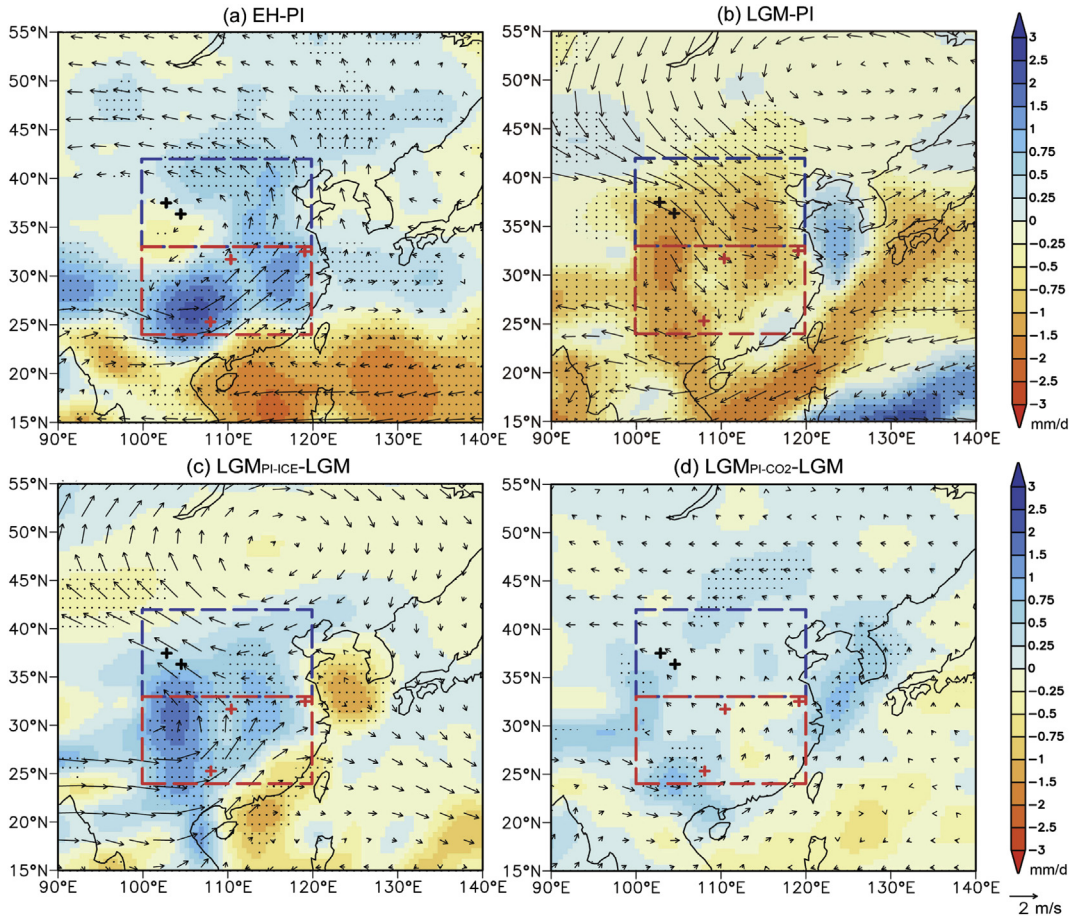

Fig. 7. CCSM3-simulated differences in summer precipitation (mm/d) and 850 hPa wind vectors (m/s) between (a) EH-PI, (b) LGM-PI, (c) $LGM_{PI\text{-}ICE}$-LGM, and (d) $LGM_{PI\text{-}CO2}$-LGM. For wind speeds, grids which are above 3000 m a.s.l. are not shown. Dashed rectangles indicate North China (NC, 33–42°N, 100–120°E) and South China (SC, 24–33°N, 100–120°N). Black and red crosses denote the location of two loess sections and three caves. Dots denote regions where the model results exceed the 95% confident level using the Student's t-test. (For interpretation of the references to color in this figure legend, the reader is referred to the web version of this article.)

impact is different from that of the ice-sheets with a rather weak magnitude under the LGM condition (Fig. 7d), because its contribution to glacial temperature anomalies is less than that of ice cover (Felzer et al., 1998). The SP percentage changes induced by decreased ice and increased CO_2 are higher in NC (13.8% and 7.4%) than in SC (9.7% and 4.9%), implying that their relative impacts are more significant in NC than in SC. Taken together, our sensitivity experiments suggest that insolation, ice and CO_2 all have played important roles in driving glacial–interglacial summer monsoon variability. Note that the insolation impact on the glacial–interglacial SP change in our sensitivity experiments is underestimated compared to the impacts of the ice-sheets and CO_2, because the insolation difference between EH and PI is lower than most of full precessional insolation cycles (Berger, 1978). Meanwhile, the impacts of ice sheets and CO_2 might be overestimated due their nonlinear response to astronomical forcing. Thus, similar to the works done by Yin et al. (2009, 2014), more sensitivity experiments together with factor separation analysis should be performed to robustly assess the individual impact of each forcing factor in the future.

5.4. Monsoon dynamics and future implication

Since the integrated effects of the astronomical and glacial factors on the summer monsoon variability are difficult to infer from modeling results or paleodata alone, we compare model results with paleo-proxies to assess the dynamics driving the summer monsoon variability (Fig. 8). Model-derived SP changes indicate that insolation forcing has greater impact on the SP change in SC than in NC, whereas the glacial forcing has weaker impact in SC compared to NC. Although the ice-sheets and CO_2 influences on the SP are spatially different, the ice effect is larger than the CO_2 effect in both regions during the LGM condition. Sensitivity coefficients of glacial and insolation impacts on the SP change are identical in SC, but change to 75% and 25% in NC, respectively. The different SP responses to astronomical and glacial forcings between NC and SC reflect the complex dynamics of the East Asia summer monsoon, linked to high- and low-latitude climates through migrations of westerly jet and subtropical High (Wu et al., 2009; Nagashima et al., 2011; Sun et al., 2012b; Chiang et al., 2015; An et al., 2015).

Model-derived summer precipitation change in NC and SC can be compared with paleo-proxies generated from Chinese loess and speleothem records (Fig. 8). Loess $\delta^{13}C_{IC}$ exhibits a smaller amplitude variability between EH and PI than between LGM and PI, consistent with the model-derived SP percentage change. This proxy-model match together with a dominant 100-ka period in our loess $\delta^{13}C_{IC}$ records indicate that glacial factors (ice and CO_2) have played a more dominant role in driving the SP changes in NC over the past 350 ka. By contrast, the speleothem $\delta^{18}O$ variability between EH and PI is more significant than the LGM-PI contrast, different from the equal percentage change of model-derived SP between EH-PI and LGM-PI. The amplitude mismatches between

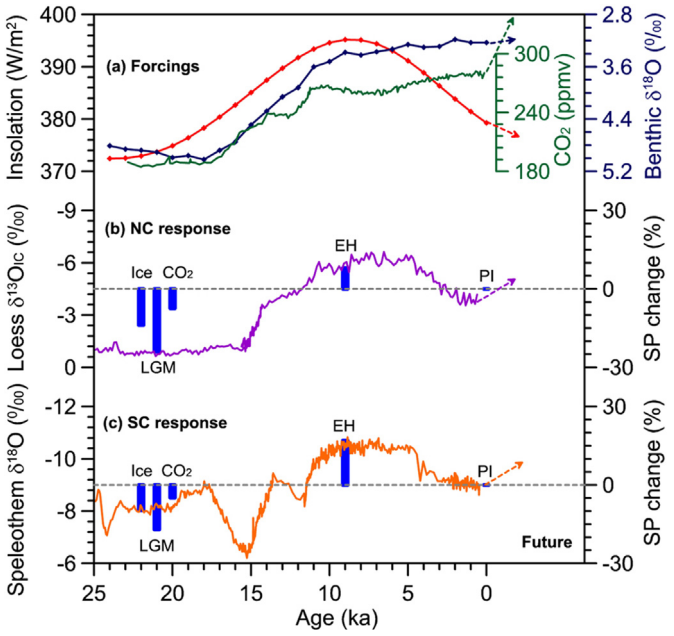

Fig. 8. Response of proxy- and model-derived summer precipitation (SP) change to insolation, ice and CO_2 forcing. (a) Natural forcings: Mean summer insolation at 65°N (red) (Berger et al., 2010), Benthic $\delta^{18}O$ stack of ice volume (dark blue) (Lisiecki and Raymo, 2005), Ice-core CO_2 (green) (Pertit et al., 1999). (b) Monsoonal response in NC: Jingyuan loess $\delta^{13}C_{IC}$ (purple line) and model-derived SP percentage changes (blue bar); (c) Monsoon response in SC: Hulu/Sanbao speleothem $\delta^{18}O$ (brown) (Wang et al., 2008b) and model-derived SP percentage changes (blue bar). Dashed arrows indicate the future trend of forcing factors and SP responses. (For interpretation of the references to color in this figure legend, the reader is referred to the web version of this article.)

speleothem $\delta^{18}O$ and insolation forcing were also evident in peak interglacials (e.g., MIS 5e, 7c and 9e), likely attributed to other factors such as changes in moisture source and related atmospheric and oceanic processes (Clemens et al., 2010; Dayem et al., 2010; Maher and Thompson, 2012; Liu et al., 2014; Cai et al., 2015).

A thorough understanding of past climate variability and dynamics, particularly regarding the CO_2 impact (Liu et al., 2012; Yin and Berger, 2012; Lu et al., 2013), would permit a robust projection of future precipitation change and a sustainable eco-societal development in monsoon-affected regions (Bradley, 2000; Berger and Loutre, 2002; Hao et al., 2012). Our data-model comparison indicates that both summer insolation as well as ice volume and CO_2 boundary conditions have played key roles in driving summer monsoon variability, though their effects on the SP changes are spatially different in East Asia. A prolonged interglacial and a delayed build-up of the northern hemisphere ice-sheets have been predicted due to the low eccentricity and the damped summer insolation variability at present (Berger et al., 1999; Berger and Loutre, 2002). Holding the CO_2 and ice-sheets constant, summer monsoon intensity would decrease slightly due to the approach of summer insolation minimum over the next few millennia (Fig. 8). However, taking into account the ongoing human-induced CO_2 emissions and the consequent global warming effects (e.g., glacial melting and sea level rise) (Meehl et al., 2012), extrapolation of our proxy-model results (i.e., 7.4% and 4.9% increases in the SP of NC and SC due to ~100 ppmv CO_2 increase) would predict increased summer precipitation over the 21st century, due to the anthropogenic CO_2 increase from 390 ppmv in 2010 to 540 ppmv in 2100 under the RCP4.5 scenario (Meinshausen et al., 2011). Our projection is consistent with strengthening of the summer monsoon in East Asia inferred from the multiple model results in the coupled model intercomparison project phase 5 (Jiang and Tian, 2013).

6. Conclusion

Investigation of a sensitive SP proxy ($\delta^{18}C_{IC}$) from two high-resolution loess sequences on the northwestern CLP reveals that the summer monsoon demonstrates significant glacial–interglacial variability, with distinct spectral peaks associated with primary astronomical periods of eccentricity (100-ka), obliquity (41-ka) and precession (23-ka). The 100-ka and 41-ka periods are predominant in the loess proxy, in contrast to a unique precessional peak in the speleothem record, implying that changing surface boundary conditions and obliquity might have played an important role in driving the summer monsoon variability. Sensitive experiments confirm that insolation, ice-sheets and CO_2 all can affect the summer precipitation change in East Asia, but with different magnitudes between NC and SC. Our work suggests that a thorough understanding of past monsoon variability and dynamics, particularly regarding the CO_2 impact, could provide increased confidence in projections of future precipitation change in monsoon-affected regions.

Acknowledgments

We thank André Berger, Qiuzhen Yin, Peter Molnar, David Battisti, Carmala Garzione, Guangshan Chen, Delia Oppo, Yanjun Cai, Xulong Wang, and Gaojun Li for commenting on the paper. Jef Vandenberghe and an anonymous reviewer are acknowledged for their valuable suggestions. This work was supported by funds from the National Basic Research Program of China (2013CB955904), the Chinese Academy of Sciences (XDB03020504 and KZZD-EW-TZ-03), and the National Science Foundation of China (40921120406 and 41472163).

Appendix A. Supplementary data

Supplementary data related to this article can be found at http://dx.doi.org/10.1016/j.quascirev.2015.03.009.

References

An, Z.S., 2000. The history and variability of the East Asian paleomonsoon climate. Quat. Sci. Rev. 19, 171–187.
An, Z.S., Clemens, S.C., Shen, J., Qiang, X.K., Jin, Z.D., Sun, Y.B., Prell, W.L., Luo, J.J., Wang, S.M., Xu, H., Cai, Y.J., Zhou, W.J., Liu, X.D., Liu, W.G., Shi, Z.G., Yan, L.B., Xiao, X.Y., Chang, H., Wu, F., Ai, L., Lu, F.Y., 2011. Glacial-interglacial Indian summer monsoon dynamics. Science 333, 719–723.
An, Z.S., Huang, Y.S., Liu, W.G., Guo, Z.T., Clemens, S., Li, L., Prell, W., Ning, Y.F., Cai, Y.J., Zhou, W.J., Lin, B.H., Zhang, Q.L., Cao, Y.N., Qiang, X.K., Chang, H., Wu, Z.K., 2005. Multiple expansions of C4 plant biomass in East Asia since 7 Ma coupled with strengthened monsoon circulation. Geology 33, 705–708.
An, Z.S., Kukla, G., Porter, S.C., Xiao, J.L., 1991. Late Quaternary dust flow on the Chinese loess plateau. Catena 18, 125–132.
An, Z.S., Wu, G.X., Li, J.P., Sun, Y.B., Liu, Y.M., Zhou, W.J., Cai, Y.J., Duan, A.M., Li, L., Mao, J.Y., Cheng, H., Shi, Z.G., Tan, L.C., Yan, H., Ao, H., Chang, H., Juan, F., 2015. Global monsoon dynamics and climate change. Annu. Rev. Earth Planet. Sci. 43, 2.1–2.49.
Berger, A., 1978. Long term variations of daily insolations and Quaternary climatic changes. J. Atmos. Sci. 35, 2362–2367.
Berger, A., Li, X.S., Loutre, M.F., 1999. Modelling northern hemisphere ice volume over the last 3 Ma. Quat. Sci. Rev. 18, 1–11.
Berger, A., Loutre, M.F., 2002. An exceptionally long interglacial ahead? Science 297, 1287–1288.
Berger, A., Loutre, M.F., Yin, Q.Z., 2010. Total irradiation during any time interval of the year using elliptic integrals. Quat. Sci. Rev. 29, 1968–1982.
Bloemendal, J., Liu, X.M., Rolph, T.C., 1995. Correlation of the magnetic susceptibility stratigraphy of Chinese loess and the marine oxygen isotope record, chronological and palaeoclimatic implications. Earth Planet. Sci. Lett. 131, 371–380.
Braconnot, P., Harrison, S.P., Kageyama, M., Bartlein, P.J., Masson-Delmotte, V., Abe-Ouchi, A., Otto-Bliesner, B., Zhao, Y., 2012. Evaluation of climate models using palaeoclimatic data. Nat. Clim. Change 2, 417–424.
Braconnot, P., Otto-Bliesner, B., Harrison, S., Joussaume, S., Peterchmitt, J.-Y., Abe-Ouchi, A., Crucifix, M., Driesschaert, E., Fichefet, Th., Hewitt, C.D., Kageyama, M., Kitoh, A., Laine, A., Loutre, M.-F., Marti, O., Merkel, U., Ramstein, G., Valdes, P., Weber, L., Yu, Y., Zhao, Y., 2007. Results of PMIP2 coupled simulations of the

mid-Holocene and Last Glacial Maximum – Part 1: experiments and large-scale features. Clim. Past 3, 261–277.
Bradley, R.S., 2000. Past global changes and their significance for the future. Quat. Sci. Rev. 19, 391–402.
Caballero-Gill, R.P., Clemens, S.C., Prell, W.L., 2012. Direct correlation of Chinese speleothem $\delta^{18}O$ and South China Sea planktonic $\delta^{18}O$: transferring a speleothem chronology to the benthic marine chronology. Paleoceanography 27, PA2203.
Cai, Y.J., Fung, I.Y., Edwards, R.L., An, Z.S., Cheng, H., Lee, J.E., Tan, L.C., Shen, C.C., Wang, X.F., Day, J.A., Zhou, W.J., Kelly, M.J., Chiang, J.C.H., 2015. Variability of stalagmite-inferred Indian monsoon precipitation over the past 252,000 y. Proc. Natl. Acad. Sci. U. S. A. http://dx.doi.org/10.1073/pnas.1424035112.
Cerling, T.E., 1984. The stable isotopic composition of modern soil carbonate and its relationship to climate. Earth Planet. Sci. Lett. 71, 229–240.
Cerling, T.E., Quade, J., Wang, Y., Bowman, J.R., 1989. Carbon isotopes in soils and paleosols as ecological and paleoecologic indicators. Nature 341, 138–139.
Chiang, J.C.H., Fung, I.Y., Wu, C.H., Cai, Y.H., Edman, J.P., Liu, Y.W., Day, J.A., Bhattacharya, T., Mondal, Y., Labrousse, C.A., 2015. Role of seasonal transitions and westerly jets in East Asian paleoclimate. Quat. Sci. Rev. 108, 111–129.
Chen, F.H., Bloemendal, J., Zhang, P.Z., Liu, G.X., 1999. An 800 ky proxy record of climate from lake sediments of the Zoige Basin, eastern Tibetan Plateau. Palaeogeogr. Palaeoecol. Palaeoclimatol. 151, 307–320.
Cheng, H., Edwards, R.L., Broecker, W.S., Denton, G.H., Kong, X., Wang, Y., Zhang, R., Wang, X., 2009. Ice age terminations. Science 326, 248–252.
Cheng, H., Sinha, A., Wang, X.F., Cruz, F.W., Edwards, R.L., 2012. The Global Paleomonsoon as seen through speleothem records from Asia and the Americas. Clim. Dyn. 39, 1045–1062.
Clemens, S.C., Prell, W.L., Sun, Y., 2010. Orbital-scale timing and mechanisms driving Late Pleistocene Indo-Asian summer monsoons: reinterpreting cave speleothem $\delta^{18}O$. Paleoceanography 25, PA4207,. http://dx.doi.org/10.1029/2010PA001926.
Collins, W.D., Bitz, C.M., Blackmon, M.L., Bonan, G.B., Bretherton, C.S., Carton, J.A., Chang, P., Doney, S.C., Hack, J.J., Henderson, T.B., Kiehl, J.T., Large, W.G., McKenna, D.S., Santer, B.D., Smith, R.D., 2006. The community climate system model version 3 (CCSM3). J. Clim. 19, 2122–2143.
Dayem, K., Molnar, P., Battistti, D.S., Roe, G.H., 2010. Lessons learned from oxygen isotopes in modern precipitation applied to interpretation of speleothem records of paleoclimate from eastern Asia. Earth Planet. Sci. Lett. 295, 219–230.
Ding, Y.H., Chan, J.C., 2005. The East Asian summer monsoon: an overview. Meteorol. Atmos. Phys. 89, 117–142.
Ding, Y.H., Wang, Z.Y., Sun, Y., 2008. Inter-decadal variation of the summer precipitation in East China and its association with decreasing Asian summer monsoon. Part I: observed evidences. Int. J. Climatol. 228, 1139–1161.
Ding, Z.L., Derbyshire, E., Yang, S.L., Yu, Z.W., Xiong, S.F., Liu, T.S., 2002. Stacked 2.6-Ma grain size record form the Chinese loess based on five sections and correlation with the deep-sea $\delta^{18}O$ record. Paleoceanography 17, 5-1.
Ding, Z.L., Liu, T., Yu, Z., Guo, Z., Zhu, R., 1995. Ice-volume forcing of East Asian winter monsoon variations in the past 800,000 years. Quat. Res. 44, 149–159.
Ding, Z.L., Yang, S.L., 2000. C3/C4 vegetation evolution over the last 7.0 Myr in the Chinese Loess Plateau: evidence from pedogenic carbonate $\delta^{13}C$. Palaeogeogr. Palaeoecol. Palaeoclimatol. 160, 291–299.
Ding, Z.L., Yu, Z.W., Rutter, N.W., Liu, T.S., 1994. Towards an orbital time scale for Chinese loess deposits. Quat. Sci. Rev. 13, 39–70.
Ding, Z.L., Yu, Z.W., Yang, S.L., Sun, J.M., Xiong, S.F., Liu, T.S., 2001. Coeval changes in grain size and sedimentation rate of eolian loess, the Chinese Loess Plateau. Geophys. Res. Lett. 28, 2097–2100.
Donohue, R.J., Roderick, M.L., McVicar, T.R., Farquhar, G.D., 2013. Impact of CO_2 fertilization on maximum foliage cover across the globe's warm, arid environments. Geophys. Res. Lett. 40, 3031–3035.
Eagle, R.A., Risi, C., Mitchell, J., Eiler, J.M., Seibt, U., Neelin, J.D., Li, G.J., Tripati, A.K., 2013. High regional climate sensitivity over continental China constrained by glacial-recent changes in temperature and the hydrological cycle. Proc. Natl. Acad. Sci. U. S. A. 110, 8813–8818.
Felzer, B., Webb III, T., Oglesby, R., 1998. The impact of ice sheets, CO_2, and orbital insolation on late Quaternary climates: sensitivity experiments with a general circulation model. Quat. Sci. Rev. 17, 507–534.
Feng, X., Epstein, S., 1995. Carbon isotopes of trees from arid environments and implications for reconstructing atmospheric CO_2 concentration. Geochim. Cosmochim. Acta 59, 2599–2608.
Frakes, L.A., Sun, J.Z., 1994. A carbon isotope record of the upper Chinese loess sequence: estimates of plant types during stadials and interstadials. Palaeogeogr. Palaeoecol. Palaeoclimatol. 108, 183–189.
Gao, Y.X., Xu, S.Y., Guo, Q.Y., Zhang, M.L., 1962. Some Problems in the East Asian Monsoon. Chinese Science Press, Beijing, pp. 49–87.
Guo, Z.T., Zhou, X., Wu, H.B., 2012. Glacial-interglacial water cycle, global monsoon and atmospheric methane changes. Clim. Dyn. 39, 1073–1092.
Han, J., Keppens, E., Liu, T., Paepe, R., Jiang, W., 1997. Stable isotope composition of the carbonate concretion in loess and climate change. Quat. Int. 37, 37–43.
Han, J.M., Lu, H.Y., Wu, N.Q., Guo, Z.T., 1996. The magnetic susceptiblity of modern soils in China and its use for paleoclimate reconstruction. Stud. Geophys. Geod. 40, 262–275.
Hao, Q.Z., Wang, L., Oldfield, F., Peng, S.Z., Qin, L., Song, Y., Xu, B., Qiao, Y.S., Bloemendal, J., Guo, Z.T., 2012. Delayed build-up of Arctic ice sheets during 400,000-year minima in insolation variability. Nature 490, 392–396.
Hays, J., Imbrie, J., Shackleton, N.J., 1976. Variations in the Earth's orbit: pacemaker of the ice ages. Science 194, 1121–1132.
Heslop, D., Langereis, C.G., Dekkers, M.J., 2000. A new astronomical timescale for the loess deposits of northern China. Earth Planet. Sci. Lett. 184, 125–139.
Hu, C.Y., Henderson, G.M., Huang, J.H., Xie, S.C., Sun, Y., Johnson, K.R., 2008. Quantification of Holocene Asian monsoon rainfall from spatially separated cave records. Earth Planet. Sci. Lett. 226, 221–232.
Huang, R.H., Chen, J.L., Huang, G., 2007. Characteristics and variations of the East Asian monsoon system and its impacts on climate disasters in China. Adv. Atmos. Sci. 26, 993–1023.
Jiang, D., Lang, X., Tian, Z., Guo, D., 2011. Last glacial maximum climate over China from PMIP simulations. Palaeogeogr. Palaeoclimatol. Palaeoecol. 309, 347–357.
Jiang, D., Tian, Z., 2013. East Asian monsoon change for the 21st century: results of CMIP3 and CMIP5 models. Chin. Sci. Bull. 58, 1427–1435.
Kukla, G., Heller, F., Liu, X.M., Xu, T.C., Liu, T.S., An, Z.S., 1988. Pleistocene climate in China dated by magnetic susceptibility. Geology 16, 811–814.
Kutzbach, J.E., Guetter, P.J., 1986. The influence of changing orbital parameters and surface boundary conditions on climate simulations for the past 18,000 years. J. Atmos. Sci. 43, 1726–1759.
Kutzbach, J.E., Liu, X., Liu, Z., Chen, G., 2008. Simulation of the evolutionary response of global summer monsoons to orbital forcing over the past 280,000 years. Clim. Dyn. 30, 567–579.
Kutzbach, J.E., Street-Perrott, F.A., 1985. Milankovitch forcing of fluctuations in the level of tropical lakes from 18 to 0 kyr BP. Nature 317, 130–134.
Li, G.J., Chen, J., Chen, Y., 2013. Primary and secondary carbonate in Chinese loess discriminated by trace element composition. Geochim. Cosmochim. Acta 103, 26–35.
Li, J.P., Zeng, Q.C., 2002. A unified monsoon index. Geophys. Res. Lett. 29, 115-1.
Li, T., Li, G.J., 2014. Incorporation of tracemetals into microcodium as novel proxies for paleo-precipitation. Earth Planet. Sci. Lett. 386, 34–40.
Lisiecki, L., Raymo, M., 2005. A Pliocene-Pleistocene stack of 57 globally distributed benthic $\delta^{18}O$ records. Paleoceanography 20, PA1003.
Liu, J., Wang, B., Cane, M.A., Yim, S.Y., Lee, J.Y., 2013. Divergent global precipitation changes induced by natural versus anthropogenic forcing. Nature 493, 656–659.
Liu, T.S., 1985. Loess and the Environment. China Ocean Press, Beijing, 174 pp.
Liu, T.S., Ding, Z.L., Rutter, N., 1999. Comparison of Milankovitch periods between continental loess and deep sea records over the last 2.5 Ma. Quat. Sci. Rev. 18, 1205–1212.
Liu, W.G., Feng, X.H., Ning, Y.F., Zhang, Q.L., Cao, Y.N., An, Z.S., 2005. $\delta^{13}C$ variation of C3 and C4 plants across an Asian monsoon rainfall gradient in arid northwestern China. Glob. Change Biol. 11, 1094–1100.
Liu, W.G., Yang, H., Sun, Y.B., Wang, X.L., 2011. $\delta^{13}C$ values of loess total carbonate: a sensitive proxy for Asian summer monsoon in arid northwestern margin of the Chinese Loess Plateau. Chem. Geol. 284, 317–322.
Liu, Z., Otto-Bliesner, B., Kutzbach, J., Li, L., Shields, C., 2003. Coupled climate simulation of the evolution of global monsoons in the Holocene. J. Clim. 16, 2472–2490.
Liu, Z.Y., Carlson, A.E., He, F., Brady, E.C., Otto-Bliesner, B.L., Briegleb, B.P., Wehrenberg, M., Clark, P.U., Wu, S., Cheng, J., Zhang, J.X., Noone, D., Zhu, J., 2012. Younger Dryas cooling and the Greenland climate response to CO_2. Proc. Natl. Acad. Sci. U. S. A. 109, 11101–11104.
Liu, Z.Y., Wen, X.Y., Brady, E.C., Otto-Bliesner, B., Yu, G., Lu, H.Y., Cheng, H., Wang, Y.J., Zheng, W.P., Ding, Y.H., Edwards, R.L., Cheng, J., Liu, W., Yang, H., 2014. Chinese cave records and the East Asia summer monsoon. Quat. Sci. Rev. 83, 115–128.
Lu, H.Y., Liu, X.D., Zhang, F.Q., An, Z.S., Dodson, J., 1999. Astronomical calibration of loess–paleosol deposits at Luochuan, central Chinese loess plateau. Palaeogeogr. Palaeoclimatol. Palaeoecol. 154, 237–246.
Lu, H.Y., Yi, S.W., Liu, Z.Y., Mason, J.A., Jiang, D.B., Cheng, J., Stevens, T., Xu, Z.W., Zhang, E.L., Jin, L.Y., Zhang, Z.H., Guo, Z.T., Wang, Y., Otto-Bliesner, B., 2013. Variation of East Asian monsoon precipitation during the past 21 k.y. and potential CO_2 forcing. Geology 41, 1023–1026.
Maher, B.A., Thompson, R., 1995. Paleorainfull reconstructions from pedogenic magnetic susceptibility variations in the Chinese loess and paleosols. Quat. Res. 44, 383–391.
Maher, B.A., Thompson, R., 2012. Oxygen isotopes from Chinese caves: records not of monsoon rainfall but of circulation regime. J. Quat. Sci. 27, 615–624.
Meinshausen, M., Smith, S.J., Calvin, K., Daniel, J.S., Kainuma, M.L.T., Lamarque, J.F., Matsumoto, K., Montzka, S.A., Raper, S.C.B., Riahi, K., Thomson, A., Velders, G.J.M., van Vuuren, D.P.P., 2011. The RCP greenhouse gas concentrations and their extensions from 1765 to 2300. Clim. Change 109, 213–241.
Meehl, G.A., Arblaster, J.M., Lawrence, D.M., Seth, A.J., Schneider, E.K., Kirtman, B.P., Min, D.H., 2006. Monsoon regimes in the CCSM3. J. Clim. 19, 2482–2495.
Meehl, G.A., Hu, A.X., Tebaldi, C., Arblaster, J.M., Washington, W.M., Teng, H.Y., Sanderson, B.M., Ault, T., Strand, W.G., White III, J.B., 2012. Relative outcomes of climate change mitigation related to global temperature versus sea level rise. Nat. Clim. Change 2, 576–580.
Nagashima, K., Tada, R.J., Tani, A., Sun, Y.B., Isozaki, Y., Toyoda, S., Hasegawa, H., 2011. Millennial-scale oscillations of the westerly jet path during the last glacial period. J. Asian Earth Sci. 40, 1214–1220.
Ning, Y.F., Liu, W.G., An, Z.S., 2006. Variation of soil $\Delta\delta^{13}C$ values in Xifeng loess-paleosol sequence and its paleoenvironmental implication. Chin. Sci. Bull. 51, 1350–1354.
Otto-Bliesner, B.L., Brady, E.C., Clauzet, G., Tomas, R., Levis, S., Kothavala, Z., 2006. Last glacial maximum and Holocene climate in CCSM3. J. Clim. 19, 2526–2544.

Pausata, F.S., Battisti, D.S., Nisancioglu, K.H., Bitz, C.M., 2011. Chinese stalagmite $\delta^{18}O$ controlled by changes in the Indian monsoon during a simulated Heinrich event. Nat. Geosci. 4, 474–480.
Peltier, W.R., 2004. Global glacial isostasy and the surface of the ice-age Earth: the ICE-5G (VM2) model and GRACE. Annu. Rev. Earth Planet. Sci. 32, 111–149.
Pertit, J.R., Jouzel, J., Raynaud, D., Barkov, N.I., Barnola, J.M., Basile, I., Bender, M., Chappellaz, J., Davis, M., Delaygue, G., Delmotte, M., Kotlyakov, V.M., Legrand, M., Lipenkov, V.Y., Lorius, C., Pépin, L., Ritz, C., Saltzman, E., Stievenard, M., 1999. Climate and atmospheric history of the past 420,000 years from the Vostok ice core, Antarctica. Nature 399, 429–436.
Porter, S.C., An, Z.S., 1995. Correlation between climate events in the North Atlantic and China during last glaciation. Nature 375, 305–308.
Prell, W.L., Kutzbach, J.E., 1992. Sensitivity of the Indian monsoon to forcing parameters and implications for its evolution. Nature 360, 647–652.
Quade, J., Cerling, T.E., Bowman, J.R., 1989a. Development of Asian monsoon revealed by marked ecological shift during the latest Miocene in northern Pakistan. Nature 342, 163–166.
Quade, J., Cerling, T.E., Bowman, J.R., 1989b. Systematic variations in the carbon and oxygen isotopic composition of pedogenic carbonate along elevation transects in the southern Great Basin. U. S. Geol. Soc. Am. Bull. 101, 464–475.
Rao, Z.G., Chen, F.H., Cheng, H., Liu, W.G., Wang, G.A., Lai, Z.P., Bloemendal, J., 2013. High-resolution summer precipitation variations in the western Chinese Loess Plateau during the last glacial. Sci. Rep. 3, 2785.
Rao, Z.G., Zhu, Z.Y., Chen, F.H., Zhang, J.W., 2006. Does $\delta^{13}C$ carb of the Chinese loess indicate past C3/C4 abundance? A review of research on stable carbon isotopes of the Chinese loess. Quat. Sci. Rev. 25, 2251–2257.
Shackleton, N.J., 2000. The 100,000-year ice-age cycle identified and found to lag temperature, carbon dioxide, and orbital eccentricity. Science 289, 1897–1901.
Sheng, X., Chen, J., Ji, J., Chen, T., Li, G., Teng, H., 2008. Morphological characters and multi-element isotopic signatures of carbonates from Chinese loess–paleosol sequences. Geochim. Cosmochim. Acta 72, 4323–4337.
Shi, Z.G., Liu, X.D., Cheng, X.X., 2012. Anti-phased response of northern and southern East Asian summer precipitation to ENSO modulation of orbital forcing. Quat. Sci. Rev. 40, 30–38.
Shi, Z.G., Liu, X.D., Sun, Y.B., An, Z.S., Liu, Z., Kutzbach, J., 2011. Distinct responses of East Asian summer and winter monsoons to astronomical forcing. Clim. Past 7, 1363–1370.
Sun, J.M., Lü, T.Y., Zhang, Z.Q., Wang, X., Liu, W.G., 2012a. Stepwise expansions of C4 biomass and enhanced seasonal precipitation and regional aridity during the Quaternary on the southern Chinese Loess Plateau. Quat. Sci. Rev. 34, 57–65.
Sun, Y.B., Clemens, S.C., An, Z.S., Yu, Z.W., 2006. Astronomical timescale and palaeoclimatic implication of stacked 3.6-Myr monsoon records from the Chinese Loess Plateau. Quat. Sci. Rev. 25, 33–48.
Sun, Y.B., Wang, X.L., Liu, Q.S., Clemens, S.C., 2010. Impacts of post-depositional processes on rapid monsoon signals recorded by the last glacial loess deposits of northern China. Earth Planet. Sci. Lett. 289, 171–179.
Sun, Y.B., Clemens, S.C., Morrill, C., Lin, X.P., Wang, X.L., An, Z.S., 2012b. Influence of Atlantic meridional overturning circulation on the East Asian winter monsoon. Nat. Geosci. 5, 46–49.
Thomas, E.K., Clemens, S.C., Prell, W.L., Herbert, T.D., Huang, Y.S., Liu, Z.Y., Damste, J.S.S., Sun, Y.B., Wen, X.Y., 2014. Temperature and leaf wax $\delta^{2}H$ records demonstrate seasonal and regional controls on Asian monsoon proxies. Geology 42, 1075–1078.
Thompson, L.G., Yao, T., Davis, M.E., Henderson, K.A., Mosley-Thompson, E., Lin, P.-N., Beer, J., Synal, H.-A., Cole-Dai, J., Bolzan, J.F., 1997. Tropical climate instability: the last glacial cycle from a Qinghai-Tibetan ice core. Science 276, 1821–1825.
Vandenberghe, J., An, Z.S., Nugtern, G., Lu, H.Y., Huissteden, K.V., 1997. New absolute time scale for the Quaternary climate in the Chinese loess region by grain-size analysis. Geology 25, 35–38.
Veizer, J., Ala, D., Azmy, K., Bruckschen, P., Buhl, D., Bruhn, F., Carden, G.A.F., Diener, A., Ebneth, S., Godderis, Y., Jasper, T., Korte, C., Pawellek, F., Podlaha, O.G., Strauss, H., 1999. 87Sr/86Sr, d13C and d18O evolution of Phanerozoic seawater. Chem. Geol. 161, 59–88.
Wang, B., Ding, Q.H., 2008. Global monsoon: dominant mode of annual variation in the tropics. Dyn. Atmos. Oceans 44, 165–183.
Wang, B., Wu, Z.W., Li, J.P., Liu, J., Chang, C.P., Ding, Y.H., Wu, G.X., 2008a. How to measure the strength of the East Asian summer monsoon. J. Clim. 21, 4449–4462.
Wang, G.A., Han, J.M., Liu, T.S., 2003. The carbon isotope composition of C3 herbaceous plants in loess area of northern China. Sci. China Earth Sci. 46, 1069–1076.
Wang, H., Follmer, L.R., 1998. Proxy of monsoon seasonality in carbon isotopes from paleosols of the southern Chinese Loess Plateau. Geology 26, 987–990.
Wang, P.X., 2009. Global monsoon in a geological perspective. Chin. Sci. Bull. 54, 1113–1136.
Wang, P.X., Clemens, S., Beaufort, L., Braconnot, P., Dickens, G.R., Huber, M., Jian, Z.M., Kershaw, P., Sarnthein, M., 2005. Evolution and variability of the Asian monsoon system: state of the art and outstanding issues. Quat. Sci. Rev. 24, 595–629.
Wang, P.X., Wang, B., Cheng, H., Fasullo, J., Guo, Z.T., Kiefer, T., Liu, Z., 2014. The global monsoon across timescales: coherent variability of regional monsoons. Clim. Past 10, 2007–2052.
Wang, Y.J., Cheng, H., Edwards, R.L., An, Z.S., Wu, J.Y., Shen, C.-C., Dorale, J.A., 2001. A high-resolution absolute-dated late Pleistocene monsoon record from Hulu Cave, China. Science 294, 2345–2348.
Wang, Y.J., Cheng, H., Edwards, R.L., Kong, X.G., Shao, X.H., Chen, S.T., Wu, J.Y., Jiang, X., Wang, X.F., An, Z.S., 2008b. Millennial- and orbital-scale changes in the East Asian monsoon over the past 224,000 years. Nature 451, 1090–1093.
Weber, S.L., Tuenter, E., 2011. The impact of varying ice sheets and greenhouse gases on the intensity and timing of boreal summer monsoons. Quat. Sci. Rev. 30, 469–479.
Webster, P.J., Magana, V.O., Palmer, T.N., Shukla, J., Tomas, R.A., Yanai, M.U., Yasunari, T., 1998. Monsoons: processes, predictability, and the prospects for prediction. J. Geophys. Res. 103, 14451–14510.
Wu, Z.W., Wang, B., Li, J.P., Jin, F.F., 2009. An empirical seasonal prediction model of the East Asian summer monsoon using ENSO and NAO. J. Geophys. Res. 114, D18120. http://dx.doi.org/10.1029/2009JD011733.
Xiao, J.L., Porter, S.C., An, Z.S., Kumai, H., Yoshikawa, S., 1995. Grain size of quartz as an indicator of winter monsoon strength on the Loess Plateau of central China during the last 130,000 yr. Quat. Res. 43, 22–29.
Yan, L.B., Liu, X.D., Zhou, Y., 2013. Variation in rainy season precipitation and associated water vapor transport over the Chinese Loess Plateau during 1961–2012. Clim. Res. 58, 43–53.
Yanase, W., Abe-Ouchi, A., 2007. The LGM surface climate and atmospheric circulation over East Asia and the North Pacific in the PMIP2 coupled model simulations. Clim. Past 3, 439–451.
Yang, S.L., Ding, Z.L., Wang, X., Tang, Z.H., Gu, Z.Y., 2012. Negative $\delta^{18}O$–$\delta^{13}C$ relationship of pedogenic carbonate from northern China indicates a strong response of C3/C4 biomass to the seasonality of Asian monsoon precipitation. Palaeogeogr. Palaeoclimatol. Palaeoecol. 317–318, 32–40.
Yin, Q.Z., Berger, A., 2012. Individual contribution of insolation and CO_2 to the interglacial climates of the past 800,000 years. Clim. Dyn. 38, 709–724.
Yin, Q.Z., Berger, A., Crucifix, M., 2009. Individual and combined effects of ice sheets and precession on MIS-13 climate. Clim. Past 5, 229–243.
Yin, Q.Z., Singh, U.K., Berger, A., Guo, Z.T., Crucifix, M., 2014. Relative impact of insolation and the Indo-Pacific warm pool surface temperature on the East Asia summer monsoon during the MIS-13 interglacial. Clim. Past 10, 1645–1657.
Zhao, Y., Harrison, S.P., 2012. Mid-Holocene monsoons: a multi-model analysis of the interhemispheric differences in the responses to orbital forcing and ocean feedbacks. Clim. Dyn. 39, 1457–1487.
Zhou, L.P., Oldfield, F., Wintle, A.G., Robinson, S.G., Wang, J.T., 1990. Partly pedogenic origin of magnetic variations in Chinese loess. Nature 346, 737–739.